

Received:
13 August 2017
Revised:
14 November 2017
Accepted:
27 November 2017

Cite as: Jiehui Jiang,
Hucheng Zhou,
Huoqiang Duan, Xin Liu,
Chuantao Zuo, Zhemin Huang,
Zhihua Yu, Zhuangzhi Yan,
The Alzheimer's Disease
Neuroimaging Initiative. A
novel individual-level
morphological brain networks
constructing method and its
evaluation in PET and MR
images.
Heliyon 3 (2017) e00475.
doi: [10.1016/j.heliyon.2017.e00475](https://doi.org/10.1016/j.heliyon.2017.e00475)



A novel individual-level morphological brain networks constructing method and its evaluation in PET and MR images

Jiehui Jiang^{a,b,*}, Hucheng Zhou^b, Huoqiang Duan^b, Xin Liu^b, Chuantao Zuo^{c,*},
Zhemin Huang^c, Zhihua Yu^{d,*}, Zhuangzhi Yan^b, The Alzheimer's Disease
Neuroimaging Initiative¹

^a Shanghai Institute for Advanced Communication and Data Science, Shanghai University, Shanghai, China

^b Institute of Biomedical Engineering, School of Communication and Information Technology, Shanghai University, Shanghai, China

^c PET Center, Huashan Hospital, Fudan University, Shanghai, China

^d Shanghai Geriatric Institute of Chinese Medicine, Shanghai, China

* Corresponding author.

E-mail addresses: jiangjiehui@shu.edu.cn (J. Jiang), zuoct_cn2000@126.com (C. Zuo), yzh1109@hotmail.com (Z. Yu).

¹ Data used in preparation of this article were obtained from the Alzheimer's Disease Neuroimaging Initiative (ADNI) database (adni.loni.usc.edu). As such, the investigators within the ADNI contributed to the design and implementation of ADNI and/or provided data but did not participate in analysis or writing of this report. A complete listing of ADNI investigators can be found at: http://adni.loni.usc.edu/wp-content/uploads/how_to_apply/ADNI_Acknowledgement_List.pdf

Abstract

Mapping the human brain is one of the great scientific challenges of the 21st century. Brain network analysis is an effective technique based on graph theory that is widely used to investigate network patterns in the human brain. Currently, mapping an individual brain network using a single image has been a hotspot in the field of brain science; techniques, such as the Kullback-Leibler (KL) method, have applications in structural Magnetic Resonance (MR) imaging. However, maintaining an image's intensity, shape, texture and gradient information during

feature extraction is very challenging. In this study, we propose a novel method for individual-level network construction based on the high-resolution Brainnetome Atlas, which shows 246 brain regions. Principal components (PCs) were obtained for each brain region using principal component analysis (PCA) for feature extraction. Individual brain networks were followed and used to construct the PC similarity measurement based on the mutual information (MI) method. To evaluate the robustness of the proposed method, three independent experiments were carried out. In the first, 34 healthy subjects underwent two Carbon 11-labeled Pittsburgh compound B Positron emission tomography (11C-PiB PET) scans; in the second, 32 healthy subjects underwent two structural MRI scans; and in the last, 10 Alzheimer's disease (AD) subjects and 10 Healthy Control (HC) subjects underwent 11C-PiB PET scans. For each subject, network metrics including clustering coefficient, path length, small-world coefficient, efficiency and node betweenness centrality were calculated. The results suggested that both the individual PET and structural MRI networks exhibited a good small-world property, and the variances within subjects was also quite small in all metrics, The average value of Coefficient of variation (CV) map was 0.33 and 0.32 for PiB PET and MR images respectively, and intra-class correlation coefficients (ICC) range from approximately 0.4 to 0.7, indicating that the new method was well adapted to the subjects. The results of intra-class correlation coefficients from the test-retest experiment were consistent with previous research employing KL divergence, but with low computational complexity. Further, differences between AD subjects and HC subjects can be observed in network metrics. The method proposed herein provides a new perspective for investigating individual brain connectivity; it would enable neuroscientists to further understand the functions of the human brain.

Keywords: Biomedical engineering, Neuroscience

1. Introduction

The human brain is one of the most complicated network systems in the world. Its complexity lies in both structure and function; it is an organic whole composed of about 10^{11} neurons and 10^{15} synapses [1]. Although the structure and function of a single neuron is relatively simple, multiple clusters of neurons and brain regions are interconnected to form a highly complex network [2]. Brain networking is one of the most important areas of neuroscience, and has gained attention world-wide as mapping the human brain has become one of the greatest scientific challenges of the 21st century [3].

Graph theory analytical methods have been widely used to analyze complex brain networks, for example to map brain network characteristics that change greatly across different cognitive functions and behaviors. In the past ten years, brain network analytical method has been extended to the study of neuropsychiatric brain

diseases, such as Alzheimer's disease (AD), schizophrenia and depression etc. For example, several studies used functional magnetic resonance imaging (fMRI) to compare the inter-regional functional connectivity between healthy and AD populations and found significantly lower clustering coefficients and path lengths in AD patients [4, 5]. A recent study from our lab employed Carbon 11-labeled Pittsburgh compound B Positron emission tomography (11C-PiB PET), one of the latest clinical technologies that detects β -amyloid plaque deposition, to reveal significant changes in the left cuneus, right caudate nucleus and left superior frontal gyrus in AD patients [6]. In addition, direct evidence from structural MRI data suggested that the coordinated patterns of cortical morphology are widely altered in AD patients [7].

Although graph theory analytical method has been successfully used to analyze various neural images, there are clear limitations of existing analytical methods. One specific limitation is that existing constructing methods, such as Pearson correlations and partial correlations, rely heavily on time series data. Networks made in this fashion are efficient for imaging data with a full time series, from scans such as EEG and fMRI. However, they are not efficient for imaging data with only one time point, such as structural Magnetic Resonance Imaging (MRI) and PET data, etc. As a result, brain networks based on structural MRI and PET data are often constructed with a set of subjects rather than one single subject [6, 8, 9, 10], which cannot explore individual brain topological organization and investigate its brain alterations or abnormalities.

More recently, in order to map an individual brain network, several investigations have been proposed. For example, Tijms et al. proposed a method to construct individual morphological networks for structural MR images. They divided the whole brain morphological networks into about 7000 nodes. Each node was composed of $3 \times 3 \times 3$ (27) voxels. Then the correlation between each two nodes was investigated [11]. Although this method realized network construction for an individual brain, the shortcoming of this method is obvious: the rigid extraction of those nodes might not optimally correspond to functionally/anatomically homogeneous regions of the brain, especially when one node was across different brain regions. To overcome above shortcoming, Kong and Wang et al. proposed the Kullback-Leibler (KL) divergence method to measure individual morphological relationships of cortical regions by calculating the KL divergence between nodes [12, 13]. This method used atlas to extract brain regions, and guaranteed functionally/anatomically homogeneity for each node. However, limitations still exist in KL method. One specific limitation is that KL method only calculated voxel intensity, and not considered deeper features, such as shape, texture and gradient features, which might not really reflect morphological organization for human brains. In addition, as one of the most time-consuming steps in network

construction, KL method took long time in calculating the connection matrix, which cannot meet clinical requirements [12, 13].

Therefore, to overcome above limitations of KL method, we propose a novel method for constructing individual brain networks by combining principal components analysis (PCA) with mutual information (MI), named PCAMI method. In this method, PCA technique was used to extract deeper features of each node. Brain network was constructed by analyzing mutual information between principal components (PC) amongst different brain regions. This article therefore is focused on two main objectives: (1) investigating whether PCAMI method is useful and robust for imaging data with only one time point, including structural MRI and PET data; and (2) validating whether PCAMI method can decrease computational complexity. To achieve above objectives, KL method was chosen and compared with PCAMI method.

2. Materials and methods

2.1. Participants

To validate the new method, three independent datasets selected from the ADNI database (<https://ida.loni.usc.edu>) were used. The first dataset included 34 Carbon 11-labeled Pittsburgh compound B Positron emission tomography (11C-PiB PET) images from health control subjects, and two PiB PET scans from each participant taken about 6 months apart. The spatial resolution of the PET scanner is $168 \times 168 \times 148$ matrices with a size of $2.0 \times 2.0 \times 1.5$ mm.

The second dataset included 32 structural MRI images from health control subjects, with two structural MRI scans from each participant taken about 1 month apart. The spatial resolution of the structural MRI is $166 \times 256 \times 256$ matrices with a size of $1.2 \times 1.0 \times 1.0$ mm. Detailed information about the magnetic resonance acquisition procedures is available at the ADNI website.

The third dataset included 20 11C-PiB PET images from 10 Alzheimer's disease and 10 health control subjects. The spatial resolution of the PET scanner is $168 \times 168 \times 148$ matrices with a size of $2.0 \times 2.0 \times 1.5$ mm.

The clinical and demographic information of the three datasets are summarized in [Table 1](#). The statistical results show that subjects did not change significantly between the two scans in the first two datasets. More information on three datasets, including ADNI number, gender information, scan times, can be found in [Supplementary materials](#).

Table 1. The clinical and demographic information of the three datasets.

Data		Gender (F/M)	Age (years)	Weight (kg)	MMSE	CDR(n)
PET (TRT)	Scan1	20F 14M	77.6 ± 6.2	71.7 ± 13.9	29.4 ± 1.2	0(30), 0.5(3), 1(1)
	Scan2	20F 14M	78.9 ± 6.1	72.5 ± 11.3	29.1 ± 1.2	0(29), 0.5(4), 1(1)
	p	1 ^a	0.40 ^b	0.78 ^b	0.37 ^b	0.79 ^b
structural MRI	Scan1	19F 13M	75.8 ± 6.7	77.6 ± 15.4	-	-
	Scan2	19F 13M	76.2 ± 6.8	77.2 ± 17.1	-	-
	p	1 ^a	0.83 ^b	0.91 ^b	-	-
PET (Comparison)	HC	6F 4M	76.3 ± 8.4	76.4 ± 9.4	30 ± 0	0(10)
	AD	5F 5M	74.7 ± 8.6	71.0 ± 11.2	17.8 ± 6.3	0.5(3),1(4),2(3)
	p	0.65 ^a	0.69 ^b	0.28 ^b	<0.001 ^b	<0.001 ^b

Note: Data is presented as the mean ± standard deviation.

F, females; M, males; n refers to the number of samples. MMSE, Mini mental state examination; CDR, Clinical Dementia Rating.

– structural MRI dataset did not provide the MMSE or CDR.

^a P-value obtained by the Pearson chi-square test.

^b P-value obtained by the two-sample two-tailed t-test.

2.2. The workflow of PCAMI method

In PCAMI method for constructing individual-level networks, there are a total of five steps: image preprocessing, extraction of the brain regions by priori atlas, feature extraction based on principal components analysis, and individual-level brain network construction based on mutual information and network analysis.

Fig. 1 shows the workflow of PCAMI method.

2.2.1. Image preprocessing

All raw images of PiB PET and MR images were in the Digital Imaging and Communications in Medicine (DICOM) format. DCM2NII (<https://www.nitrc.org/projects/dcm2nii/>) was used to convert images from the DICOM to NIfTI format. The transformed images were preprocessed using Statistical Parametric Mapping 8 (SPM8) implemented in Matlab2014a.

2.2.1.1. (a) PiB PET image preprocessing

First, each PET image was spatially normalized to the Montreal Neurological Institute (MNI, McGill University, Montreal, Canada) space using the ‘Normalize: Estimate and Write’ function. In this step, the individual images were spatially warped to a reference PET template from SPM software. This spatial warping is an automated procedure that uses affine transformation with 12 parameters. Then, the

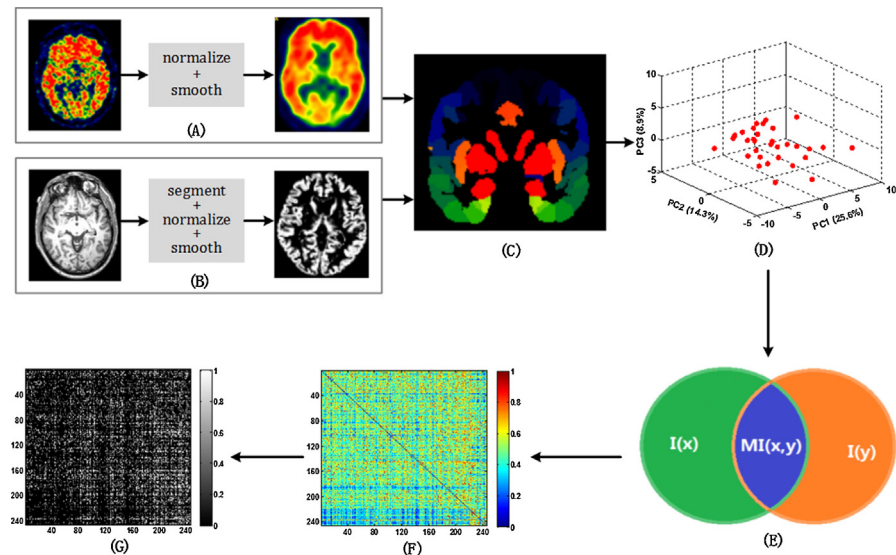


Fig. 1. The workflow of PCAMI method proposed in this study. (A) PiB PET image preprocessing; (B) MR image preprocessing; (C) brain region extraction using priori atlas Brainnetome; (D) Principal components analysis for each region; (E) Similarity measurement based on mutual information between components; (F) MI-based connectivity matrix for each subject; (G) Binary matrix transformed from MI matrix.

normalized images were smoothed by convolution using an isotropic Gaussian kernel with $8 \times 8 \times 8 \text{ mm}^3$ as the FWHM to increase signal to noise ratio for statistical analysis. Finally, the images were transferred to gray level images with a grayscale of [0,255].

2.2.1.2. (b) MR image preprocessing

First, the native MR images were registered into stereotaxic space by applying rigid-body transformations. Second, the registered images were segmented into gray matter (GM), white matter (WM), and cerebrospinal fluid (CSF) tissue probability maps with priori tissue maps as a reference through a unified segmentation algorithm. The density map was provided by International Consortium for Brain Mapping (ICBM), which provided the probability distribution of GM, WM and CSF in standard spatial $2 \times 2 \times 2 \text{ mm}^3$. Then, the GM images were spatially normalized to the standard MNI space. Finally, the normalized GM images were smoothed with $5 \times 5 \times 5 \text{ mm}^3$ FWHM, as defined in the SPM8 manual, to improve the images' noise-signal ratio in order to reducing the impact of noise on the results.

2.2.2. Extracting the brain regions using priori atlas

According to graph theory, a network consists of vertices and edges that connect a sequence of vertices. Therefore, to construct the brain network, the first step is

defining the network nodes. In this study, a high-resolution Brainnetome Atlas was chosen to define network nodes. The Brainnetome Atlas was developed by Fan et al. in 2016 [14]; it includes 210 cortical and 36 subcortical regions, and it contains information on both anatomical and functional connections. Hence all of the PiB PET and MR images in this study were linearly registered by the Brainnetome Atlas with a same size as $91 * 109 * 91$ pixels, and were finally divided into 246 nodes.

2.2.3. Feature extraction based on principal components analysis

After extracting the brain regions, principal components analysis (PCA) was performed for feature reduction and de-correlation. Compared to traditional feature extraction methods used in clinics, such as voxel values and standardized uptake values (SUV), PCA methods can successfully address three issues existing in traditional methods by defining image details. First, each brain region contains hundreds of voxels in high dimensions. These voxels are usually relatively small, which leads to the curse of dimensionality. Second, because the voxels in a brain region are highly correlated, it is necessary to conduct de-correlation. Third, not only intensity information, but also shape, texture and gradient information from the image are important. PCA, a popular statistical procedure in data analysis, transforms the high dimensional data to a new coordinate system in lower dimensional space through an orthogonal transformation. The data in the new coordinate system represents the principal components (PCs) and features of the original data. Therefore, PCA method can effectively identify the most important features and structures in the image, such as edges and textures, while PCA method can remove noise and redundancy, and reduce the original image data dimensionality simultaneously [15, 16].

In this study, PCA was performed for each area separately after extracting the brain regions, and PCs of each area were obtained. Six detailed steps of this process can be explained as follows:

- (a) The brain regions of all subjects were organized into matrix \mathbf{X} , with n rows and m columns, where n represents the number of the subjects, m represents the number of the brain regions. Because Brainnetome Atlas template was used in this study, m is equal to 246. x_{ij} is a vector representing the feature dimensions of the j -th brain region of the i -th subject.

$$\mathbf{X} = \begin{bmatrix} x_{11} & x_{12} & \cdots & x_{1m} \\ x_{21} & x_{22} & \cdots & x_{2m} \\ \vdots & \vdots & \vdots & \vdots \\ x_{n1} & x_{n2} & \cdots & x_{nm} \end{bmatrix} = [x_1, x_2, \cdots, x_m]$$

$$x_i = [x_{1i} \quad x_{2i} \quad \cdots \quad x_{ni}]^T, i = 1, 2, \dots, m$$

- (b) The matrix X is de-mean normalized by columns through subtraction of the mean value of each row, where X_0 represents the de-mean normalized X .

$$X_0 = \begin{bmatrix} x_1 - \text{mean}(x_1) \\ x_2 - \text{mean}(x_2) \\ \vdots \\ x_m - \text{mean}(x_m) \end{bmatrix}^T$$

- (c) Computing the covariance matrix of the de-mean normalized X .
- (d) Computing the eigenvalues, D , and the corresponding eigenvectors, V , of the covariance matrix.
- (e) Rearranging the eigenvectors from large to small according to the corresponding eigenvalues.
- (f) Multiplying the eigenvectors by X_0 to obtain the PCs.

After extracting the brain regions, PCA was performed for both the PET and MR images in this study. The mathematical models of PCA showed that the number of principal components in each brain region was equal to the number of subjects minus 1 [17]. As a result, from PCA of the PiB PET data, 33 principal components (PCs) were obtained for each brain region, representing the most relevant image information (intensity, texture, and shape). Similarly, for structural MRI data, each brain region contained 31 PCs, which represent the most relevant image information of structural MR images.

2.2.4. Brain network construction based on mutual information method

Mutual information (MI) was proposed in this step to define the inter-regional relations between nodes. In information theory, the amount of information provided by an event should be a function of the probability that the event occurs, and can be defined as follows:

$$I(x) = f(p(x))$$

where $p(x)$ represents the probability of an event and $I(x)$ represents the amount of information provided by the event. Mathematically, the relationship between $I(x)$ and $p(x)$ has been strictly defined as follows:

$$I(x) = -\log p(x)$$

The marginal entropy and joint entropy were defined as follows, represent the mathematical expectation of $I(x)$:

$$H(x) = -\sum_x p(x) \log p(x)$$

$$H(x, y) = -\sum_x \sum_y p(x, y) \log p(x, y)$$

Then, the mutual information of two random variables is a measure of the mutual dependence between the two variables. More specifically, mutual information is used to measure the amount of information obtained about one random variable through the other random variable, which can be defined as follows:

$$MI(x, y) = H(x) + H(y) - H(x, y)$$

Namely,

$$MI(x, y) = -\sum_x p(x) \log p(x) - \sum_y p(y) \log p(y) + \sum_x \sum_y p(x, y) \log p(x, y)$$

To calculate the probability density functions $p(x)$, kernel density estimate (KDE) with a normal kernel was performed; this is a nonparametric method for estimating probability densities [18].

In this step, similarity measurement for mutual information between PCs was performed, giving definitive connection strength between the brain regions. Three sub-steps were used. In the first, PCs of each two different regions were denoted as x and y ; then probability density functions $p(x)$ and $p(y)$ were calculated based on PCs x and y respectively; and finally $MI(x, y)$ was calculated by definition formula. As a result, a size of 246×246 MI-based connectivity matrix was achieved for each subject.

2.2.5. Network analysis

Then, the sparsity threshold method was applied to binarized the networks. Because there is no definitive way to select a single threshold, a wide range of sparsity thresholds were applied and the network parameters were calculated at each threshold. Using a previous study, a sparsity threshold range of 6% – 40% was chosen with an interval of 1% [6, 19, 20].

After defining the threshold range, the MI matrix was transformed into a binary matrix that was then described as a network. In the binary matrix, an element of 1 indicates that there is a connection between two nodes, and 0 indicates that there is no connection, as shown in Fig. 1(F), (G).

In this study, the following network metrics were calculated: clustering coefficient (C), characteristic path length (L), gamma, lambda, small-world coefficient (sigma), local efficiency (localE), global efficiency (globalE), and node betweenness centrality (BC). All parameters were calculated using the open toolkit GREYNA (<https://www.nitrc.org/projects/gretna/>) [21] and The Brain Connectivity Toolbox (BCT, <http://www.nitrc.org/projects/bct/>) [22].

In the graph theory, the C of a network is as a measure of the degree to which nodes in a graph tend to cluster together [23]. The L is as a measure of the efficiency of the information or the mass transport of a network [8]. A small-world network should meet the following criteria: $\gamma \gg 1$, $\lambda \approx 1$ and $\sigma > 1$ [24, 25]. The globalE and localE are as the measure of how efficiently it exchanges information in entire network and local network, respectively [26]. BC is typically used to determine the number of candidate hubs in a network [27]. According to previous studies, nodes with b_i (equal to $BC/\text{averaged BC}$) values greater than the averaged betweenness value are considered as candidate hubs of the network.

2.3. Evaluation of PCAMI method

2.3.1. Coefficient of variation (CV)

After obtaining the MI-based connectivity matrices, the coefficient of variation across the subjects were calculated to evaluate the consistency. The coefficient of variation (CV), also known as relative standard deviation (RSD), is an important statistic for measuring the variability of the observed values in the data, and can be defined as the ratio of the standard deviation to the mean value:

$$CV = \frac{\sigma}{\mu} * 100\%$$

where σ represents the standard deviation of the population, μ represents the mean value of the population. In this study, referring to previous literature [12, 13], we assumed that the difference between HCs' brains were small in both structural MRI and PET images. Hence, CV across subjects was used to measure robustness of PCAMI Method [13].

2.3.2. Test-retest (TRT) reliability analysis

A test-retest (TRT) reliability analysis was performed to evaluate whether the new method proposed in this study is repeatable. Specifically, intra-class correlation coefficients (ICC) were calculated, which represents the ratio of between-subject variance to total variance, defined as follows:

$$ICC = \frac{\delta_{between}^2}{\delta_{between}^2 + \delta_{within}^2}$$

where $\delta_{between}^2$ and δ_{within}^2 represents total variance that is “between groups” and “within groups”. In general, an ICC value below 0.4 is considered poor reliability, 0.4–0.58 is considered fair, 0.59–0.75 is considered good reliability, and greater than 0.75 is considered excellent [28, 29]. In this study, ICC was calculated to perform the test-retest reliability between the first and second scans

based on MI-based connectivity matrices without binarization for both PET and MRI images.

2.4. Comparison of PCAMI method and present methods

In order to investigate whether PCAMI method is viable, direct comparison with the KL divergence method was performed. Differences between the network metrics from the two methods, such as C, L, gamma, lambda, sigma, localE, globalE were calculated. Two-sample T-Test was used to analyze statistical differences of PCAMI method and KL method.

Computing consuming for both methods were also compared in the computing platform Windows 7 64-bit OS with an 8 G memory and quad-core Intel[®] processors that operates at 3.2 GHz.

2.5. Comparison of network metrics between AD and HC subjects by using PCAMI method

To further demonstrate the potential clinical values of the proposed method, we used a dataset including 20 11C-PiB PET images from 10 Alzheimer's disease and 10 health control subjects. The individual brain network for each subject based on the proposed method was set up and the network parameters were calculated, respectively. Finally, all network metrics between Alzheimer's disease and health control subjects were compared.

3. Results

3.1. CV Map across subjects

Fig. 2 shows the resulting CV map for the first scan of PiB PET (Fig. 2A) and MR images (Fig. 2B). As can be observed across subjects, the CV map exhibited small variation throughout the brain. The average value of CV map was 0.33 and 0.32 for PiB PET and MR images, respectively.

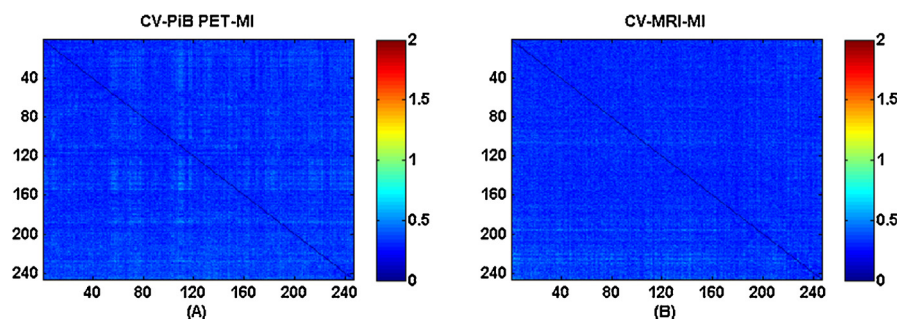


Fig. 2. (A) CV map across the subjects for the first scan of PiB PET data determined using the method proposed; (B) CV map for the first scan of structural MRI data determined using the method proposed.

3.2. Individual network metrics of two scans in PiB PET and MR images

In this study, the network metrics C, L, gamma, lambda and sigma were generated for each subject. Fig. 3 shows the mean values and standard deviations of each scan across subjects determined using the method proposed in this study. Compared with random networks, both the individual PiB PET and structural MRI networks exhibited larger values in the clustering coefficient and approximately equal values in path length.

Over the entire threshold range of 6% – 40%, both the PiB PET and structural MRI networks fulfilled $\gamma \gg 1$, which satisfied the small-world network criterion.

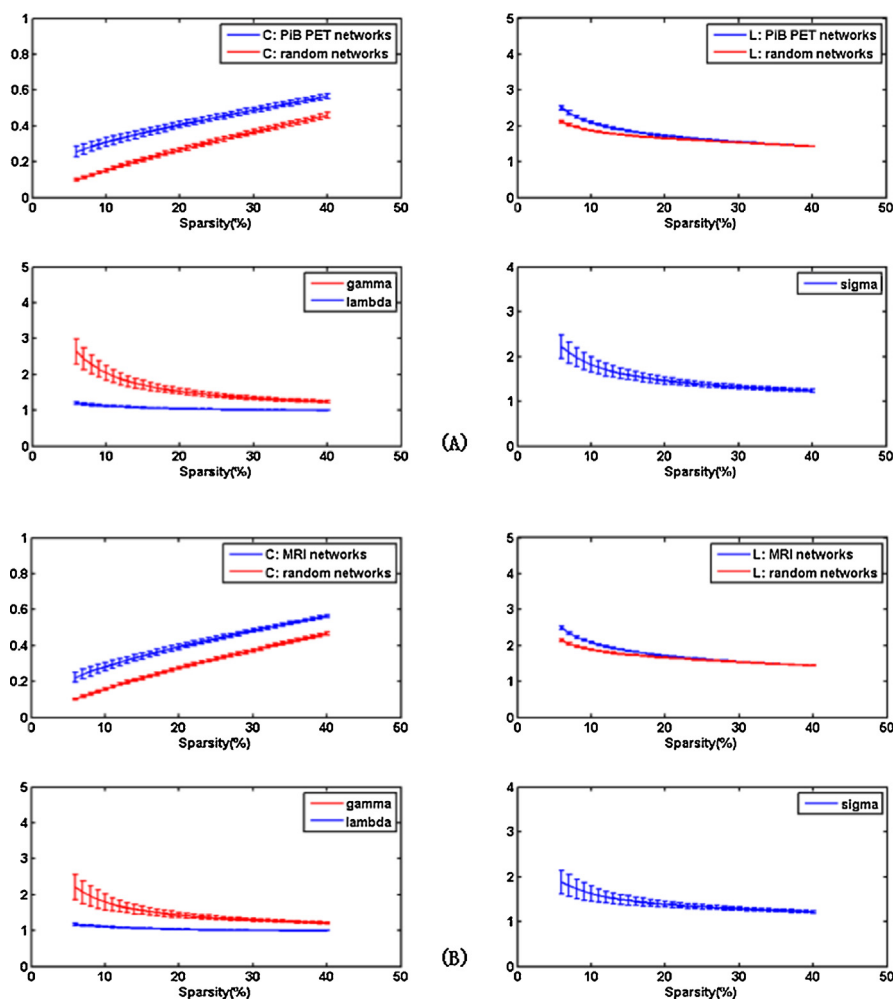


Fig. 3. Network metrics of the first scan data from PiB PET and structural MRI scans by using the new method proposed in this study. The x-axis represents the sparsity threshold ranges from 6% to 40% with 1% steps. The y-axis represents the values of network metrics. The error bars indicate the standard deviation within subjects. (A) Network metrics of PiB PET images; (B) Network metrics of structural MRI images.

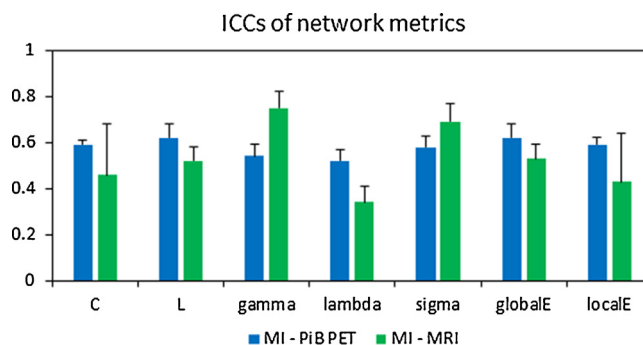
Table 2. The minimum, maximum and mean values of gamma, lambda and sigma across the entire thresholds.

	PiB PET			structural MRI		
	gamma	lambda	sigma	gamma	lambda	sigma
minimum	1.23	1.00	1.23	1.21	1.00	1.21
maximum	2.63	1.19	2.21	2.20	1.17	1.88
mean	1.58	1.05	1.49	1.47	1.04	1.40

Table 2 shows the minimum, maximum and mean values of gamma, lambda and sigma across the entire thresholds. Specifically, the subjects demonstrate a favorable small-world property in both the PiB PET and structural MRI networks when using PCAMI method proposed in this study. These findings are consistent with previous research showing that the human brain is a small-world network. Further, the variances within each subject are quite small in all metrics (Fig. 3). This suggests that the proposed method is subjectively adaptive.

3.3. Test-retest reliability of the individual network

A TRT reliability analysis was performed to assess the robustness of the method proposed in the present study. Fig. 4 shows the average values and standard deviations of the ICC of network metrics across the threshold range. Overall, the ICCs of PiB PET and structural MRI networks range from approximately 0.4 to 0.7. For example, across the threshold range, the mean ICC value of the clustering coefficient and path length of the PiB PET network was 0.59 and 0.62, respectively. These TRT results indicate that the method for constructing individual PiB PET and structural MRI networks achieved fair or excellent reliability.

**Fig. 4.** The mean ICCs of network metrics. The error bars represent the standard deviation across the threshold range.

3.4. Regression analysis for the two scans

When assessing a newly proposed method, it is important that it can obtain consistent results between two scans conducted at two different time points. Therefore, linear regression analysis for the two scans was carried out to investigate the consistence of network metrics. Figs. 5 and 6 show the linear regression results of the PiB PET and structural MRI networks, respectively. To evaluate the performance of the regression analysis, the R^2 statistic and p value were calculated, as these are regarded as two of the most important statistical indicators in regression analysis. As expected, for all metrics, the results of R^2 statistic were about 0.99 and p values were below 10^{-3} , demonstrating that the two scans exhibited an excellent linear relationship. Specifically, using the network metrics of the first scan, the results of the second scan can be reliably predicted, suggesting that the method for constructing individual PiB PET and structural MRI networks can achieve extremely consistent results across at least two scans.

3.5. Hubs of the individual PiB PET and structural MRI Networks

In order to determine the hubs, a fixed sparsity of 18% was chosen according to our previous study [6]. Several hub nodes were identified in the PiB PET and structural MRI network at the fixed sparsity of 18% by calculating the network parameter of betweenness centrality (nodes with normalized betweenness centrality values with greater than average betweenness value plus one standard deviation). Fig. 7 shows the hub nodes in the sagittal view. Using the PiB PET images, 41 and 36 hub nodes were identified for the first and second scan, respectively. Among those hub nodes, 12 were found in both scans, including the insular gyrus, medio-ventral occipital cortex, lateral occipital cortex, amygdala, hippocampus and thalamus. Table 3 lists the 12 hub regions and their normalized bi values. Using the structural MRI

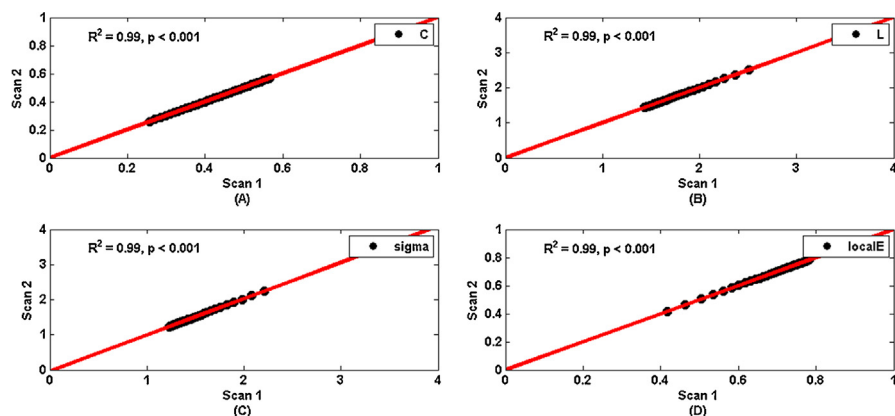


Fig. 5. Linear regression analysis of the PiB PET network metrics. (A) clustering coefficient; (B) path length; (C) small-world coefficient; (D) local efficiency.

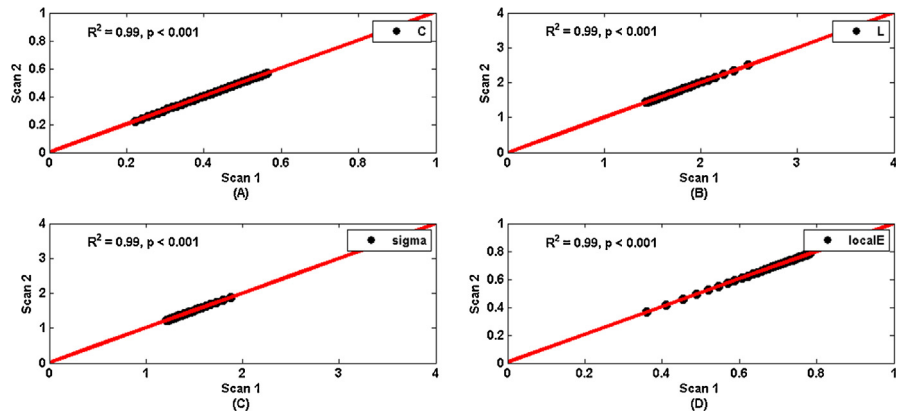


Fig. 6. Linear regression analysis of the structural MRI network metrics. (A) clustering coefficient; (B) path length; (C) small-world coefficient; (D) local efficiency.

images, 38 and 39 hub nodes were identified for the first and second scans, respectively. 16 hubs were identified in both scans, including the orbital gyrus, fusiform gyrus, precuneus, insular gyrus, cingulate gyrus, medio-ventral occipital cortex, lateral occipital cortex, amygdala, hippocampus, basal ganglia and thalamus, as reported in Table 4. The hubs found in both PiB PET and structural MRI networks have been reported at least once in previous studies.

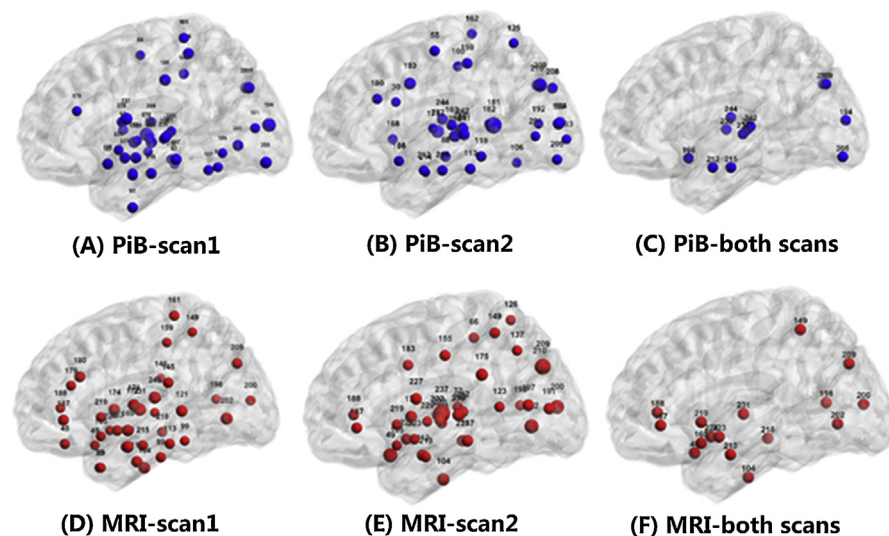


Fig. 7. Network hubs in PiB PET and structural MRI networks. Marker size denotes hub importance. (A) The identified hubs in the first PiB PET scan images; (B) Hubs identified in the second PiB PET scan images; (C) The hubs identified in both PiB PET scan images; (D) Hubs identified in the first structural MRI scan images; (E) Hubs identified in the second structural MRI scan images; (F) The hubs identified in the both structural MRI scan images. The hub nodes were visualized using the BrainNet Viewer package [30].

Table 3. Hubs of PiB PET data identified in both scans.

region no.	region	bi		MNI coordinates (mm)		
		scan1	scan2	x	y	z
166	INS_R_6_2	1.43	1.25	33	14	-13
194	MVOcC_R_5_3	1.75	1.38	8	-90	12
205	LOcC_L_4_4	1.46	1.29	-30	-88	-12
209	LOcC_L_2_2	1.46	1.73	-22	-77	36
210	LOcC_R_2_2	1.43	1.41	29	-75	36
212	Amyg_R_2_1	1.28	1.28	19	-2	-19
215	Hipp_L_2_1	1.38	1.31	-22	-14	-19
232	Tha_R_8_1	1.72	1.66	7	-11	6
236	Tha_R_8_3	1.22	1.50	18	-22	3
240	Tha_R_8_5	1.27	1.29	15	-25	6
242	Tha_R_8_6	1.28	1.51	13	-27	8
244	Tha_R_8_7	1.31	1.42	10	-14	14

Table 4. Hubs of structural MRI data identified in both scans.

region no.	region	bi		MNI coordinates (mm)		
		scan1	scan2	x	y	z
49	OrG_L_6_5	1.27	1.73	-10	18	-19
104	FuG_R_3_1	1.55	1.52	33	-15	-34
149	PCun_L_4_2	1.25	1.34	-8	-47	57
165	INS_L_6_2	1.30	1.25	-32	14	-13
187	CG_L_7_7	1.45	1.33	-4	39	-2
188	CG_R_7_7	1.29	1.31	5	41	6
198	MVOcC_R_5_5	1.28	1.28	15	-63	12
200	LOcC_R_4_1	1.33	1.70	34	-86	11
202	LOcC_R_4_2	1.60	1.74	48	-70	-1
209	LOcC_L_2_2	1.40	1.95	-22	-77	36
213	Amyg_L_2_2	1.55	1.30	-27	-4	-20
218	Hipp_R_2_2	1.37	1.43	29	-27	-10
219	BG_L_6_1	1.30	1.28	-12	14	0
223	BG_L_6_3	1.39	1.27	-17	3	-9
224	BG_R_6_3	1.24	1.35	15	8	-9
231	Tha_L_8_1	1.66	1.29	-7	-12	5

3.6. Comparison between PCAMI method and present methods

The difference between network metrics of the PCAMI method and KL divergence method can be seen in Fig. 8. The differences between the metrics from the two methods were in an acceptable range. For instance, the differences between sigma values were lower than 0.5 across the entire threshold, indicating that the new framework proposed is feasible for constructing individual PiB PET and structural MRI networks, and has the potential to describe the human brain network with small-world and high-efficiency characteristics.

Table 5 shows the results of statistical differences in network metrics between two methods. All parameters of network metrics show significant statistical difference ($p < 0.05$) except sigma values in four scans and gamma value in the first PiB PET scan. That means PCAMI method has essential distinction for constructing brain network in comparison to KL method.

To evaluate the robustness of the method, all of the PiB PET and structural MRI data were manually selected to ensure two PET or structural MRI scans were performed for each participant, and to ensure that two evaluation experiments, including CV mapping across the subjects and ICC of the network metrics, were performed and compared with the KL method.

Fig. 9 shows the results of CV mapping of the PiB PET and structural MRI networks using the KL divergence. Compared with the KL method, the CV map obtained from the present method demonstrated relatively low CV values for both the PiB PET and structural MRI networks. Specifically, for the PiB PET network, the average value of the CV map was 0.33 with the present method, while it was a much higher 0.56 using KL method. For the structural MRI network, the average value of the CV map was 0.32 with the present method and similarly, was 0.37 using the KL method. These findings suggest that the present method exhibits considerably better consistency across participants.

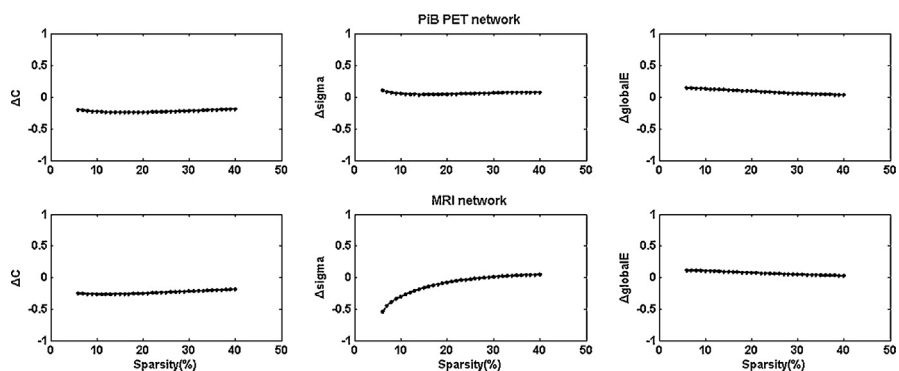


Fig. 8. The network metric differences between the present method and the KL divergence method.

Table 5. Statistical differences of network metrics between PCAMI method and KL method.

P	C	L	gamma	lambda	sigma	globalE	localE
First_structural MRI scan	0	0.0042	0.0092	0	0.1083a	0.0041	0
First_PiB PET scan	0	0.0013	0.4319a	0	0.3435a	0.001	0
Second_structural MRI scan	0	0.0035	0.0107	0	0.1543a	0.0031	0
Second_PiB PET scan	0	0.0017	0.516	0	0.2268a	0.0014	0

^arepresents haven't a statistically significant difference ($p < 0.05$).

The comparison of ICCs between the present method and KL divergence method is shown in Fig. 10. Overall, the ICC results from the present method were similar to the results that were obtained using KL divergence method. For the PiB PET network, the present method demonstrated better ICC values in path length and global efficiency. For the structural MRI network, the present method demonstrated a better ICC values in path length, gamma, sigma, global efficiency and local efficiency.

In summary, the new method proposed in this study exhibited an acceptable robustness when compared with the KL method, suggesting its potential to serve as a method for brain network construction at an individual level.

Furthermore, the time requirements for the present method and KL method were recorded and compared. Using the KL method, it took 61 minutes for individual network construction per participant. However, in the same operating environment, only 23 minutes were needed for each participant using the present method, which suggests lower computational complexity compared to the KL method. This time efficiency is mainly due to PCA reducing the dimension of the original image data.

3.7. Comparison of network metrics between AD and HC subjects by using PCAMI method

Fig. 11 shows comparison results of network metrics between AD and HC groups at different sparsity from 6% to 40%. It can be found that the network metrics of C,

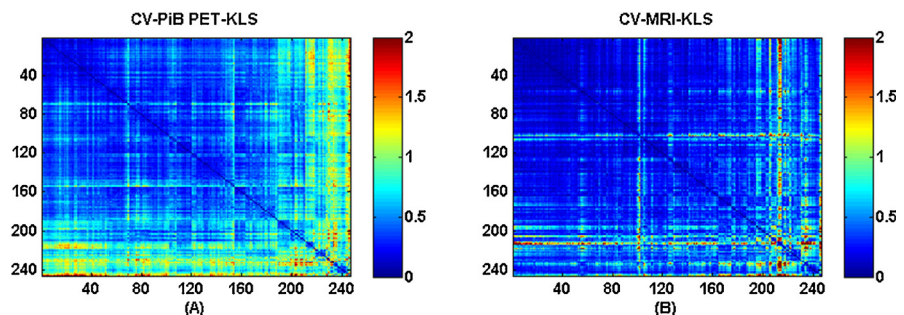


Fig. 9. (A) CV map across the subjects for the first scan of PiB PET data constructed using the KL method; (B) CV map for the first scan of structural MRI data constructed using the KL method.

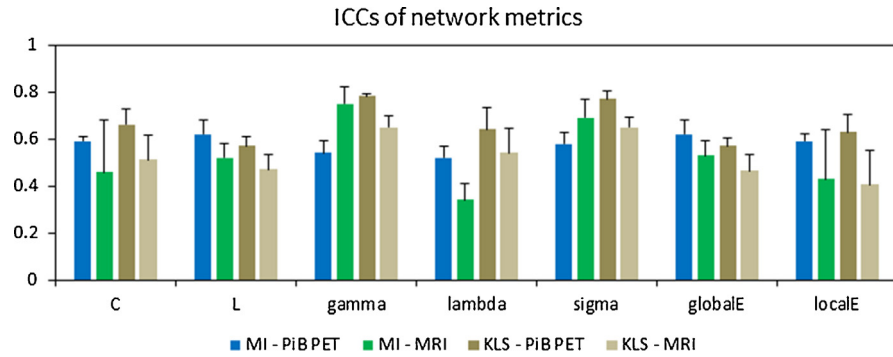


Fig. 10. Comparison of ICCs between the present method and KL divergence method.

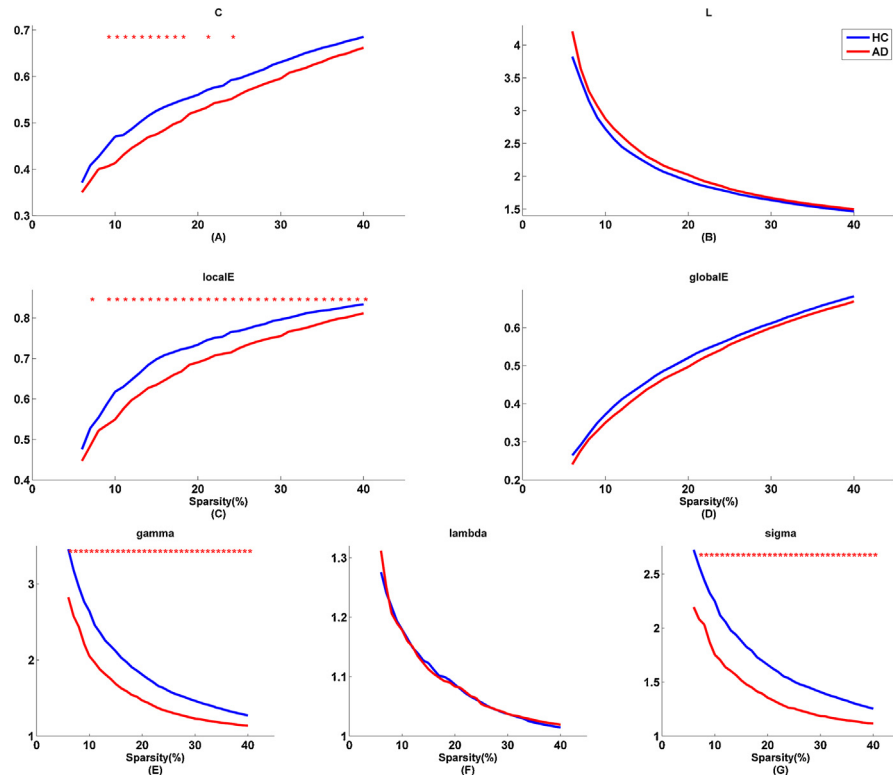


Fig. 11. Comparisons of network metrics between AD and HC groups based on 11C-PiB PET images. (A) C, clustering coefficient; (B) L, characteristic path length; (C) localE, local efficiency; (D) globalE, global efficiency; (E) gamma parameters; (F) lambda parameters; (G) sigma parameters. The x-axis represents the sparsity threshold ranges from 6% to 40% with 1% steps. The y-axis represents the values of network metrics. The red curve represents the average of corresponding network parameters across subjects in AD groups and the blue curve represents the average of corresponding network parameters across subjects in HC groups. Asterisks (*) show significant differences (two-sample two-tailed t-test, $p < 0.05$).

localE, gamma were lower in the AD group than in the HC group. Especially, a decrease in sigma was obvious in the AD group, indicating the loss of small-world characteristics was observed in the AD group compared to the HC group.

Significant differences for network metrics were assessed using two-sample two-tailed t-test ($p < 0.05$). Significant differences in C, localE, gamma, and sigma were found at the corresponding sparsity thresholds between AD and HC groups, but not be found in L, globalE and lambda (Fig. 11).

4. Discussion

Mapping individual brain networks has been a research hotspot in recent years. Although there have been a few studies that have proposed methods for constructing single-subject morphological brain networks, such as KL method, limitations still exist. Two limitations of KL method are proposed from previous studies: (1) KL method only calculated voxel intensity, and not considered deeper features, such as shape, texture and gradient features, which might not really reflect morphological organization for human brains; (2) the computing consuming of KL method cannot meet clinical requirements. This paper proposed a novel PCAMI method to solve above limitations. This is the first time that a novel method for mapping individual brain networks based on PCA for feature extraction and mutual information for individual-level network construction has been proposed and applied to PiB PET and structural MR images according to our knowledge.

4.1. Innovative aspects of PCAMI method

PCA and MI are two innovations in PCAMI method to solve limitations of existing single-subject morphological brain networks constructing methods.

First, in most previous studies, similarity measurements between regions were based only on voxel intensity of the images [9, 10, 31, 32]. However, maintaining the shape, texture and gradient information of the image during feature extraction is a great challenge. In this study, we innovatively used the PCA method for image feature extraction, then the brain network was constructed based on these features, rather than voxel intensity. As a statistical procedure that uses an orthogonal transformation to convert original data into a set of linearly uncorrelated variables called principal components, PCA function is mostly used as a tool in exploratory data analysis. In this study, PCs well obtained the most relevant shape, texture and gradient information of structural MRI and PET images besides voxel intensity.

Second, MI was proposed for defining the inter-regional relations between nodes after feature extraction. Compared to traditional correlation coefficient approaches using the kernel density function, such as KL method, MI can better handle non-

Table 6. Comparison of network metrics between the present study and previous studies.

Study	Imaging		N ^a	C	L	gamma	lambda	sigma
Present study	PET		246	0.39	1.77	1.59	1.05	1.51
	structural MRI			0.37	1.76	1.47	1.04	1.41
[8]	structural MRI	Pearson correlation coefficients	54	-	-	~ 1.1	~ 1	~ 1.1
[7]	structural MRI	partial correlation coefficients	90	~ 0.22	~ 1.8	~ 1.4	~ 1	~ 1.4
[12]	structural MRI	KL divergence	90	~ 0.6	~ 2.3	~ 2.4	~ 1.2	~ 1.8
[30]	fMRI	Pearson correlation coefficients	90	~ 0.51	~ 1.9	~ 2	~ 1.1	~ 1.8
[33]	fMRI	Pearson correlation coefficient	90	~ 0.3	~ 1.7	~ 1.5	~ 1.1	~ 1.4
[10]	PET	partial correlation analysis	90	~ 0.55	~ 2.1	-	-	-
[9]	PET	Partial Correlation Analysis	90	~ 0.45	~ 2.1	~ 1.4	~ 1.05	~ 1.3

a: N represents the number of network nodes.

- represents unreported information.

linear relationships. Hence MI is used in PCAMI method because correlations between PCs amongst brain regions are non-linear.

4.2. Effectiveness of network metrics from PCAMI method

To validate whether network metrics of both HCs' structural MRI and PiB PET scans from PCAMI method are effective, we compared clustering coefficient (C), characteristic path length (L), gamma, lambda, small-world coefficient (sigma), local efficiency (localE) and global efficiency (globalE) between PCAMI method and methods from literature, including KL method for individual subjects, and Pearson correlation coefficients and Partial correlation coefficients for a group of subjects.

Table 6 shows comparison results between the present network metrics and other previous studies at a fixed threshold of 18%. These results of other previous studies are mainly based on classical brain network constructing method for a group of subjects, such as Pearson correlations and partial correlations. The results of network metrics from this study were similar to those of previous studies. In addition, the small-world property was observed in this study in both PiB PET and structural MRI networks, which is consistent with previous studies.

4.3. Hub regions

In the field of network science, nodes positioned to make strong contributions to global network function are referred to as network hubs [34]. Using the present method, 12 network hubs were identified in the PET network and 16 hubs were identified in the structural MRI network. Almost all of the hubs have been

previously reported as biomarkers. For example, the thalamus region was identified as hub node of the PET network in this study. According to a recent study, the thalamus region is a critical hub that could function to integrate heteromodal information and maintain the modular structure of cortical functional networks [35]. In addition, another study used diffusion imaging techniques to construct connection maps covering the entire cortical surface, and found that provincial hubs are members of occipital modules [36]. Similarly, the occipital region was identified as a hub of the structural MRI network in the present study. As a whole, these results indicate that the hub regions identified in this study are indeed physiologically significant, and illustrate the potential application of our proposed method, given the fact that hub regions are generally altered in various brain disorders, such as Alzheimer's disease and schizophrenia. Therefore, the potential of hub regions serving as imaging markers for disease diagnosis is an interesting topic for future research.

4.4. Potential clinical application values of PCAMI method

To evaluate potential clinical application values of the proposed method, a direct comparison experiment between the AD group and the HC group was carried out. The comparison results in Fig. 11 showed that differences of network metrics between two groups were obvious, indicating that PCAMI method may be useful to distinguish diseases in clinics. In addition, the results of Fig. 11 can also be observed in previous literature. For instance, several scholars [5, 37, 38] supposed that small-worldness were lost in AD group because Alzheimer-related pathology would result in randomized brain networks [39]. A decrease clustering in the AD group could also be found [39, 40], etc.

4.5. Limitations and further considerations

There are several issues in this study that still need to be further considered. First, high-resolution Brainnetome Atlas was used in this study for the first time. There are many other brain atlases available, such as AAL template and Harvard-Oxford atlas et al. Whether a different atlas would have an impact on the results is still not known. In the future, a direct comparison among various atlases is needed.

Second, PCA is a statistical procedure that uses an orthogonal transformation to convert original data into a set of linearly uncorrelated variables called PCs. Same PCs (e.g., 1st PC) amongst different brain regions was equal. Hence MI method can be used to analyze PCs. Nevertheless, the significance of different PCs within same brain regions was unclear. It is still unknown how much intensity, shape, texture and gradient features are included in each PC, and what the weight functions of features were in each PC. More studies are needed to further

investigate the meaning of the features, as well as relationships of different PCs within same brain regions.

Third, and most importantly, the PCA analysis can only be performed on a group of subjects. Therefore, the PCAMI method proposed in this study did not fully achieve the goal of constructing an individual-level brain network, and there is still much improvement needed in future work.

Fourth, although both structural MR and PiB PET image data were analyzed, whether the resolutions of different imaging modalities will affect calculation efficiency of construction brain network needs further study. Finally, we need to further investigate potential clinical application value of the proposed method to distinguish different brain disorder diseases (such as Alzheimer's disease and Parkinson's disease dementia) in different imaging modalities.

5. Conclusion

In summary, the current study proposed a new method that was based on PCA for feature extraction and MI for connection definition, to explore the individual-level brain network using PiB PET and structural MR images. There are a total of five steps in the new method: image preprocessing, extraction of the brain regions by priori atlas, feature extraction based on principal components analysis, and individual-level brain network construction based on mutual information and network analysis. Overall, the new method demonstrates considerable consistency and robustness, and would provide a new perspective in understanding the functional and structural connectivity of the human brain.

Declarations

Author contribution statement

Jiehui Jiang: Conceived and designed the experiments; Analyzed and interpreted the data; Wrote the paper.

Hucheng Zhou, Huoqiang Duan, Xin Liu: Contributed reagents, materials, analysis tools or data; Performed the experiments; Wrote the paper.

Chuantao Zuo, Zhemin Huang, Zhihua Yu, Zhuangzhi Yan: Analyzed and interpreted the data; Wrote the paper.

The Alzheimer's Disease Neuroimaging Initiative: Contributed reagents, materials, analysis tools or data.

Funding statement

This research was supported by National Science Foundation of China (No. 61603236, No. 81671239, No. 81361120393, No. 81401135), Research funding from Shanghai Technology and Science key project in healthcare (No.17441902100, 17ZR1427700, ZYKC201602002), the development fund for Shanghai talents (No. 201448) and Shanghai Key Laboratory of Psychotic Disorders (No.13dz2260500). Data collection and sharing for this project was funded by the Alzheimer's Disease Neuroimaging Initiative (ADNI) (National Institutes of Health Grant U01 AG024904) and DOD ADNI (Department of Defense award number W81XWH-12-2-0012). ADNI is funded by the National Institute on Aging, the National Institute of Biomedical Imaging and Bioengineering, and through generous contributions from the following: AbbVie, Alzheimer's Association; Alzheimer's Drug Discovery Foundation; Araclon Biotech; BioClinica, Inc.; Biogen; Bristol-Myers Squibb Company; CereSpir, Inc.; Eisai Inc.; Elan Pharmaceuticals, Inc.; Eli Lilly and Company; EuroImmun; F. Hoffmann-La Roche Ltd and its affiliated company Genentech, Inc.; Fujirebio; GE Healthcare; IXICO Ltd.; Janssen Alzheimer Immunotherapy Research & Development, LLC.; Johnson & Johnson Pharmaceutical Research & Development LLC.; Lumosity; Lundbeck; Merck & Co., Inc.; Meso Scale Diagnostics, LLC.; NeuroRx Research; Neurotrack Technologies; Novartis Pharmaceuticals Corporation; Pfizer Inc.; Piramal Imaging; Servier; Takeda Pharmaceutical Company; and Transition Therapeutics. The Canadian Institutes of Health Research is providing funds to support ADNI clinical sites in Canada. Private sector contributions are facilitated by the Foundation for the National Institutes of Health (www.fnih.org). The grantee organization is the Northern California Institute for Research and Education, and the study is coordinated by the Alzheimer's Disease Cooperative Study at the University of California, San Diego. ADNI data are disseminated by the Laboratory for Neuro Imaging at the University of Southern California.

Competing interest statement

The authors declare no conflict of interest.

Additional information

Supplementary content related to this article has been published online at <http://dx.doi.org/10.1016/j.heliyon.2017.e00475>.

Acknowledgements

The authors would like to thank Mr. Xinghui Shu for his kindly help with data preprocessing.

References

- [1] D. Kuzum, R.G.D. Jeyasingh, B. Lee, H.-S.P. Wong, Nanoelectronic programmable synapses based on phase change materials for brain-inspired computing, *Nano Lett.* 12 (2012) 2179–2186.
- [2] O. Sporns, G. Tononi, G.M. Edelman, Connectivity and complexity: the relationship between neuroanatomy and brain dynamics, *Neural Netw.* 13 (2000) 909–922.
- [3] B.M. Altevogt, S.L. Hanson, A.I. Leshner, Molecules to Minds: Grand Challenges for the 21st Century, *Neuron* 60 (2008) 406–408.
- [4] E.J. Sanz-Arigitia, M.M. Schoonheim, J.S. Damoiseaux, S.A.R.B. Rombouts, E. Maris, F. Barkhof, P. Scheltens, C.J. Stam, Loss of 'Small-World' Networks in Alzheimer's Disease: Graph Analysis of fMRI Resting-State Functional Connectivity, *PLoS One* 5 (2010) e13788.
- [5] K. Supekar, V. Menon, D. Rubin, M. Musen, M.D. Greicius, Network Analysis of Intrinsic Functional Brain Connectivity in Alzheimer's Disease, *PLoS Comput. Biol.* 4 (2008) e1000100.
- [6] H. Duan, J. Jiang, J. Xu, H. Zhou, Z. Huang, Z. Yu, Z. Yan, Alzheimer's Disease Neuroimaging Initiative, Differences in A β brain networks in Alzheimer's disease and healthy controls, *Brain Res.* 2017 (1655) 77–89.
- [7] Y. He, Z. Chen, A. Evans, Structural insights into aberrant topological patterns of large-scale cortical networks in Alzheimer's disease, *Alzheimers & Dementia the Journal of the Alzheimers Association* 4 (2008) 4756–4766.
- [8] Y. He, Z.J. Chen, A.C. Evans, Small-World Anatomical Networks in the Human Brain Revealed by Cortical Thickness from MRI, *Cereb. Cortex* 17 (2007) (1991) 2407–2419.
- [9] Z. Liu, L. Ke, H. Liu, W. Huang, Z. Hu, Changes in topological organization of functional PET brain network with normal aging, *PLoS One* 9 (2014) e88690.
- [10] E.H. Seo, D.Y. Lee, J.M. Lee, J.S. Park, B.K. Sohn, D.S. Lee, Y.M. Choe, J.I. Woo, Whole-brain functional networks in cognitively normal, mild cognitive impairment, and Alzheimer's disease, *PLoS One* 8 (2013) e53922.
- [11] B.M. Tijms, P. Series, D.J. Willshaw, S.M. Lawrie, Similarity-based extraction of individual networks from gray matter MRI scans, *Cereb. Cortex* 22 (2012) (1991) 1530–1541.

- [12] X.-z. Kong, Z. Liu, L. Huang, X. Wang, Z. Yang, G. Zhou, Z. Zhen, J. Liu, Mapping individual brain networks using statistical similarity in regional morphology from MRI, *PLoS One* 10 (2015) e0141840.
- [13] H. Wang, X. Jin, Y. Zhang, J. Wang, Single-subject morphological brain networks: connectivity mapping, topological characterization and test–retest reliability, *Brain Behav.* 6 (2016).
- [14] L. Fan, H. Li, J. Zhuo, Y. Zhang, J. Wang, L. Chen, Z. Yang, C. Chu, S. Xie, A.R. Laird, P.T. Fox, S.B. Eickhoff, C. Yu, T. Jiang, The Human Brainnetome Atlas: A New Brain Atlas Based on Connectional Architecture, *Cereb. Cortex* 26 (2016) (1991) 3508–3526.
- [15] H. Bingham, Random projection in dimensionality reduction: applications to image and text data. Proceedings of the seventh ACM SIGKDD international conference on Knowledge discovery and data mining, ACM (2001) 245–250.
- [16] M. Chawla, PCA and ICA processing methods for removal of artifacts and noise in electrocardiograms: A survey and comparison, *Appl. Soft Comput.* 11 (2011) 2216–2226.
- [17] I.T. Jolliffe, Principal component analysis and factor analysis, *Principal Component Analysis* (2002) 150–166.
- [18] Y.-I. Moon, B. Rajagopalan, U. Lall, Estimation of mutual information using kernel density estimators, *Phys. Rev. E* 52 (1995) 2318.
- [19] M. Göttlich, T.F. Münte, M. Heldmann, M. Kasten, J. Hagenah, U.M. Krämer, Altered resting state brain networks in Parkinson's disease, *PLoS One* 8 (2013) e77336.
- [20] Z. Yao, Y. Zhang, L. Lin, Y. Zhou, C. Xu, T. Jiang, Alzheimer's Disease Neuroimaging Initiative, Abnormal cortical networks in mild cognitive impairment and Alzheimer's disease, *PLoS Comput. Biol.* 6 (2010) e1001006.
- [21] J. Wang, X. Wang, M. Xia, X. Liao, A. Evans, Y. He, GREYNA: a graph theoretical network analysis toolbox for imaging connectomics, *Front. Hum. Neurosci.* 9 (2015).
- [22] M. Rubinov, O. Sporns, Complex network measures of brain connectivity: uses and interpretations, *NeuroImage* 52 (2010) 1059–1069.
- [23] H. Inoue, Y.-Y. Liu, Revealing the intricate effect of collaboration on innovation, *PLoS One* 10 (2015) e0121973.
- [24] S. Maslov, K. Sneppen, Specificity and stability in topology of protein networks, *Science* 296 (2002) 910–913.

- [25] D.J. Watts, S.H. Strogatz, Collective dynamics of small-world networks, *Nature* 393 (1998) 440–442.
- [26] V. Latora, M. Marchiori, Efficient Behavior of Small-World Networks, *Phys. Rev. Lett.* 87 (2001) 1–4.
- [27] E. Bullmore, O. Sporns, Complex brain networks: graph theoretical analysis of structural and functional systems, *Nat. Rev. Neurosci.* 10 (2009) 186.
- [28] C.M. Bennett, M.B. Miller, How reliable are the results from functional magnetic resonance imaging? *Ann. NY Acad. Sci.* 1191 (2010) 133–155.
- [29] J.-H. Wang, X.-N. Zuo, S. Gohel, M.P. Milham, B.B. Biswal, Y. He, Graph Theoretical Analysis of Functional Brain Networks: Test-Retest Evaluation on Short- and Long-Term Resting-State Functional MRI Data, *PLoS One* 6 (2011) e21976.
- [30] M. Xia, J. Wang, Y. He, BrainNet Viewer: a network visualization tool for human brain connectomics, *PLoS One* 8 (2013) e68910.
- [31] J. Wang, L. Wang, Y. Zang, H. Yang, H. Tang, Q. Gong, Z. Chen, C. Zhu, Y. He, Parcellation-dependent small-world brain functional networks: a resting-state fMRI study, *Hum. Brain Mapp.* 30 (2009) 1511–1523.
- [32] X. Zhao, Y. Liu, X. Wang, B. Liu, Q. Xi, Q. Guo, H. Jiang, T. Jiang, P. Wang, Disrupted small-world brain networks in moderate Alzheimer's disease: a resting-state FMRI study, *PLoS One* 7 (2012) e33540.
- [33] J. Zhang, J. Wang, Q. Wu, W. Kuang, X. Huang, Y. He, Q. Gong, Disrupted Brain Connectivity Networks in Drug-Naive, First-Episode Major Depressive Disorder, *Biol. Psychiatry* 70 (2011) 334–342.
- [34] M.P. van den Heuvel, O. Sporns, Network hubs in the human brain, *Trends Cogn. Sci.* 17 (2013) 683–696.
- [35] K. Hwang, M.A. Bertolero, W. Liu, M. Esposito, The human thalamus is an integrative hub for functional brain networks, *bioRxiv* (2016).
- [36] P. Hagmann, L. Cammoun, X. Gigandet, R. Meuli, C.J. Honey, V.J. Wedeen, O. Sporns, Mapping the Structural Core of Human Cerebral Cortex, *PLoS Biol.* 6 (2008) e159.
- [37] L.R. Peraza, J.-P. Taylor, M. Kaiser, Divergent brain functional network alterations in dementia with Lewy bodies and Alzheimer's disease, *Neurobiol. Aging* 36 (2015) 2458–2467.

- [38] C.J. Stam, B.F. Jones, G. Nolte, M. Breakspear, P. Scheltens, Small-world networks and functional connectivity in Alzheimer's disease, *Cereb. Cortex* 17 (2007) 92.
- [39] C.J. Stam, W. De Haan, A. Daffertshofer, B.F. Jones, I. Manshanden, A.M.v. C.v Walsum, T. Montez, J.P. Verbunt, J.C. De Munck, B.W. Van Dijk, Graph theoretical analysis of magnetoencephalographic functional connectivity in Alzheimer's disease, *Brain* 132 (2009) 213.
- [40] B.M. Tijms, C. Möller, H. Vrenken, A.M. Wink, W. de Haan, W.M. van der Flier, C.J. Stam, P. Scheltens, F. Barkhof, Single-subject grey matter graphs in Alzheimer's disease, *PLoS One* 8 (2013) e58921.